Supplementary Information for

Anomalous ultrafast heat transfer in single palladium nanocrystals seen with an X-ray free electron laser

David Yang[1*], James Wrigley[2], Jack Griffiths[1], Longlong Wu[1†], Ana F. Suzana[1‡], Jiecheng Diao[3§], Angel Rodriguez-Fernandez[2], Joerg Hallmann[2], Alexey Zozulya[2], Ulrike Boesenberg[2], Roman Shayduk[2], Jan-Etienne Pudell[2], Anders Madsen[2], Ian K. Robinson[1,3*]

[1]Condensed Matter Physics and Materials Science Department, Brookhaven National Laboratory, Upton, NY, 11973, United States.

[2]European X-Ray Free-Electron Laser Facility, Holzkoppel 4, 22869 Schenefeld, Germany.

[3]London Centre for Nanotechnology, University College London, London, WC1E 6BT, United Kingdom.

[†]Present address: Shanghai Advanced Research Institute, Chinese Academy of Sciences, Shanghai, 201210, China

[‡]Present address: Chemical Sciences and Engineering Division, Argonne National Laboratory, Lemont, IL, 60439, United States.

[§]Present address: Center for Transformative Science, ShanghaiTech University, Shanghai, 201210, China

[*]Corresponding author. Email: dyang2@bnl.gov, i.robinson@ucl.ac.uk

This PDF file includes:

Supplementary Text

Peak oscillation fitting

The oscillations in horizontal peak position in Fig. 3a were fitted using an empirical damped sinusoidal function with amplitude modulation at the troughs, shown in Eq. S1,

$$\begin{aligned} s(\tau) &= A_1 \cos\left(\frac{2\pi\tau}{T_1} + \phi_1\right) \\ S_p(\tau) &= \left[A_1 + \text{rectifier}(s(\tau)) \cdot A_2 \cos\left(\frac{2\pi\tau}{T_2} + \phi_2\right)\right] \cdot \\ & \quad e^{-\lambda\tau} + C, \text{ where} \\ \text{rectifier}(s(\tau)) &= \begin{cases} 1 & \text{if } s(\tau) < 0, \\ 0 & \text{otherwise, and} \end{cases} \end{aligned} \tag{S1}$$

where τ is the delay time, A_1 and A_2 are the amplitudes, T_1 and T_2 are the periods, ϕ_1 and ϕ_2 are the phase shifts, λ is the damping constant, and C is the offset. The subscripts 1 and 2 refer to the variables for the signal and modifier, respectively. The fit parameters are shown in Table S1.

The oscillations of the FWHM of the fitted Bragg peak for crystal A are captured in Fig. 3 d. These oscillations are fitted with a damped sinusoidal function, shown in Eq. S2,

$$S_w(\tau) = B \cos\left(\frac{2\pi\tau}{P} + \beta\right) e^{-\zeta\tau} + D, \tag{S2}$$

where B is the amplitude, P is the period, β is the phase shift, ζ is the damping constant, and D is the offset. The fit parameters are shown in Table S2.

Crystal rotation

Fig. S6 shows that there is no consistency in the rotation direction for each crystal. This can be attributed to the local arrangement of nanocrystal neighbours, which would have been different for each of our measured nanocrystals.

The rotation for crystal A with respect to the rocking axis is estimated in Fig. S7. The measured rocking curve of the diffraction peak is a direct measure of how rapidly the intensity drops off with angle. When there is a change in average lattice parameter, there will be a

deviation of Bragg angle, $\Delta\theta$. The theta deviation for 170 mJ/cm^2 in Fig. S7b is $\sim 0.035\ ^\circ$ at around 40 ps. The theta angle for the Pd 111 reflection is 17.9 °. Thus, the expected ΔQ for this deviation is determined by,

$$\begin{aligned} \Delta Q &= \frac{4\pi}{\lambda}\left[\sin\left(\theta - \Delta\theta\right) - \sin\left(\theta\right)\right] \\ \Delta Q &= \frac{4\pi}{1.377602\ \text{Å}}\left[\sin\left(17.9\ ^\circ - 0.035\ ^\circ\right) - \sin\left(17.9\ ^\circ\right)\right] \\ \Delta Q &= 0.0053\ \text{Å}^{-1} \end{aligned} \tag{S3}$$

At negative delay time in Fig. 3a, $Q_0 = 2.8038\ \text{Å}^{-1}$. Thus, $Q_0 - \Delta Q = 2.7985\ \text{Å}^{-1}$, which agrees with Q at around 40 ps in Fig. 3a.

For 230 mJ/cm^2 in Fig. S7b, $\Delta\theta \approx 0.050\ ^\circ$ at around 40 ps. Thus, the expected ΔQ for this deviation is determined by,

$$\begin{aligned} \Delta Q &= \frac{4\pi}{\lambda}\left[\sin\left(\theta - \Delta\theta\right) - \sin\left(\theta\right)\right] \\ \Delta Q &= \frac{4\pi}{1.377602\ \text{Å}}\left[\sin\left(17.9\ ^\circ - 0.050\ ^\circ\right) - \sin\left(17.9\ ^\circ\right)\right] \\ \Delta Q &= 0.0076\ \text{Å}^{-1} \end{aligned} \tag{S4}$$

At negative delay time in Fig. 3a, $Q_0 = 2.8038\ \text{Å}^{-1}$. Thus, $Q_0 - \Delta Q = 2.7962\ \text{Å}^{-1}$, which is reasonably expected for 230 mJ/cm^2 at around 40 ps in Fig. 3a. Thus, the rotation at high laser fluences can be explained as due to the average lattice expanding and contracting. This noticeably changes the intensity of the Bragg peak of crystal A at 170 mJ/cm^2 and 230 mJ/cm^2.

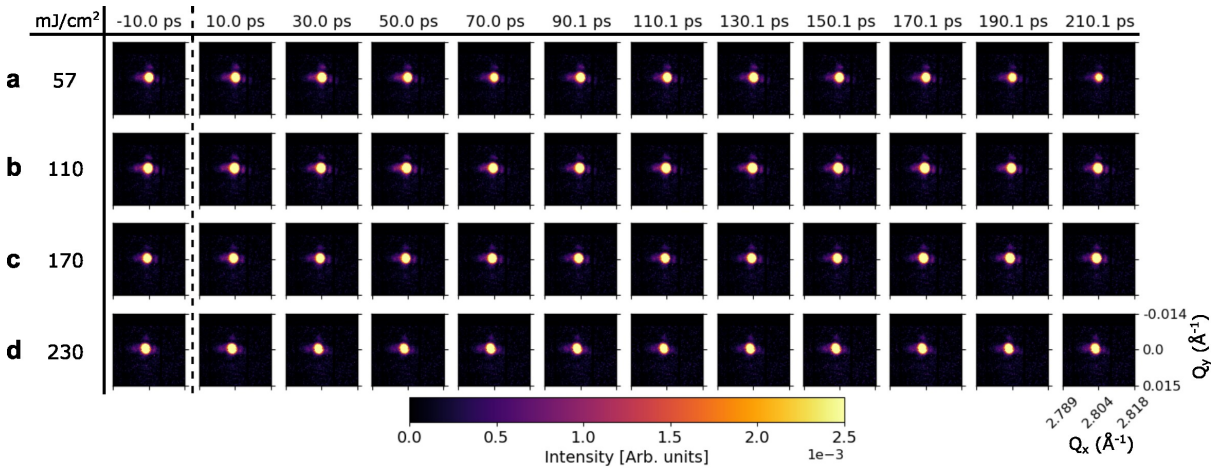

Figure S1: The unpumped pulses of the 111 Bragg peak intensity on a linear scale for crystal A at various delay times and laser fluences. Rows **a** - **d** correspond to sequential delay measurements using different fluences.

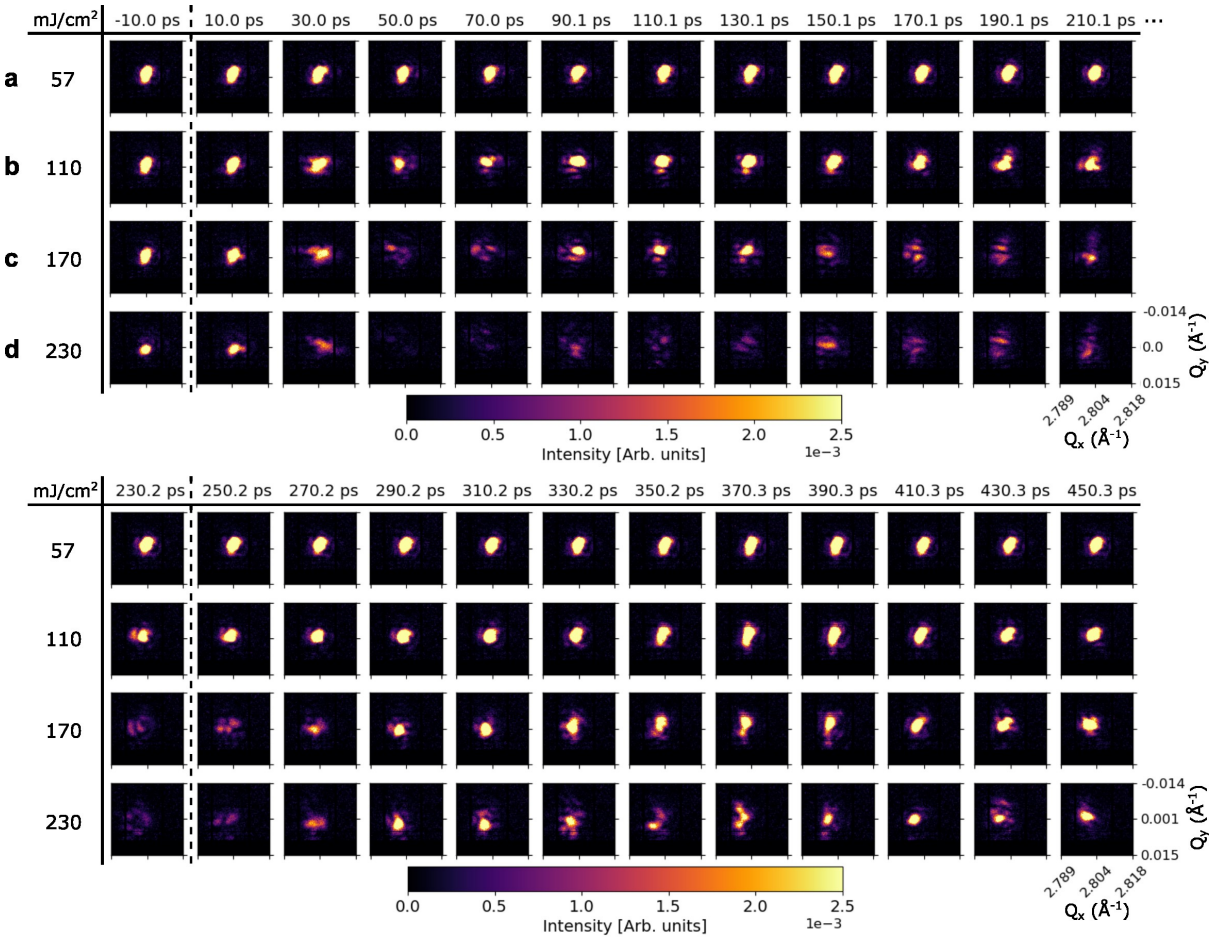

Figure S2: Evolution of the 111 Bragg peak intensity on a linear scale for crystal B at various delay times and laser fluences. Rows **a** - **d** correspond to sequential delay measurements using different fluences.

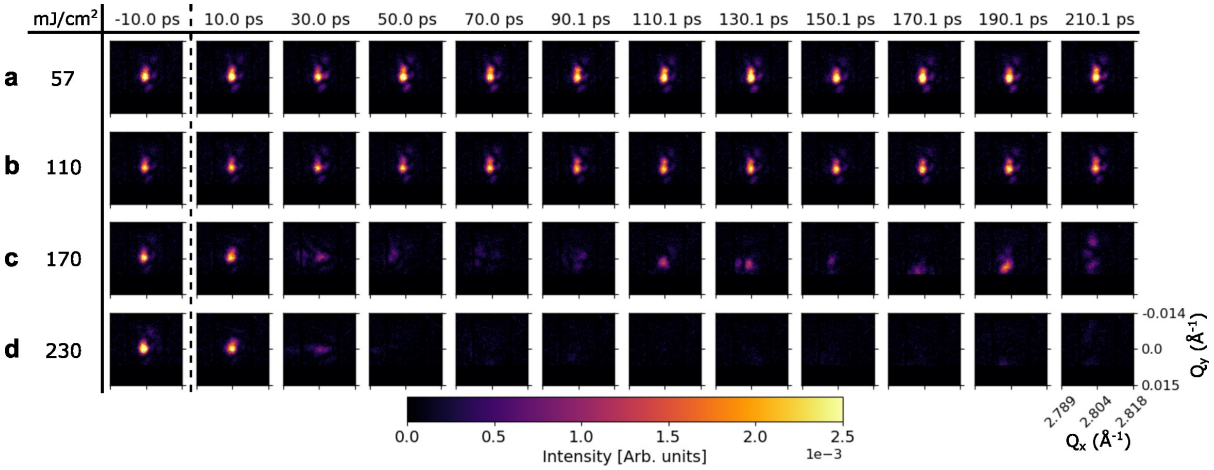

Figure S3: Evolution of the 111 Bragg peak intensity on a linear scale for crystal C-1 at various delay times and laser fluences. Rows **a** - **d** correspond to sequential delay measurements using different fluences.

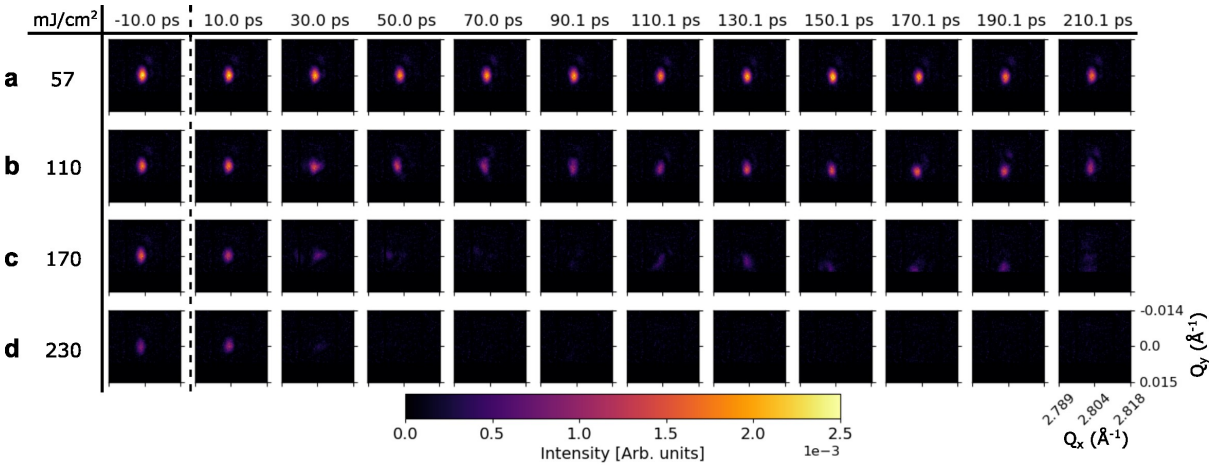

Figure S4: Evolution of the 111 Bragg peak intensity for on a linear scale crystal C-2 at various delay times and laser fluences. Rows **a** - **d** correspond to sequential delay measurements using different fluences.

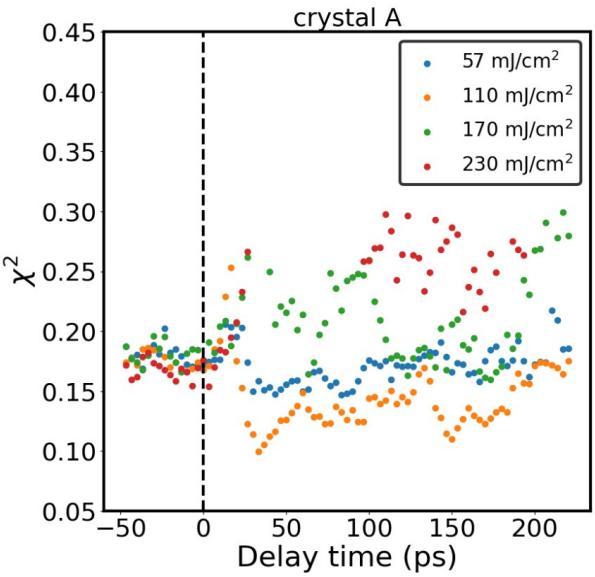

Figure S5: The χ^2 error of the Gaussian fit of the Bragg peak at various delay times and laser fluences. Each point corresponds to the fits shown in Fig. 3a and S6a.

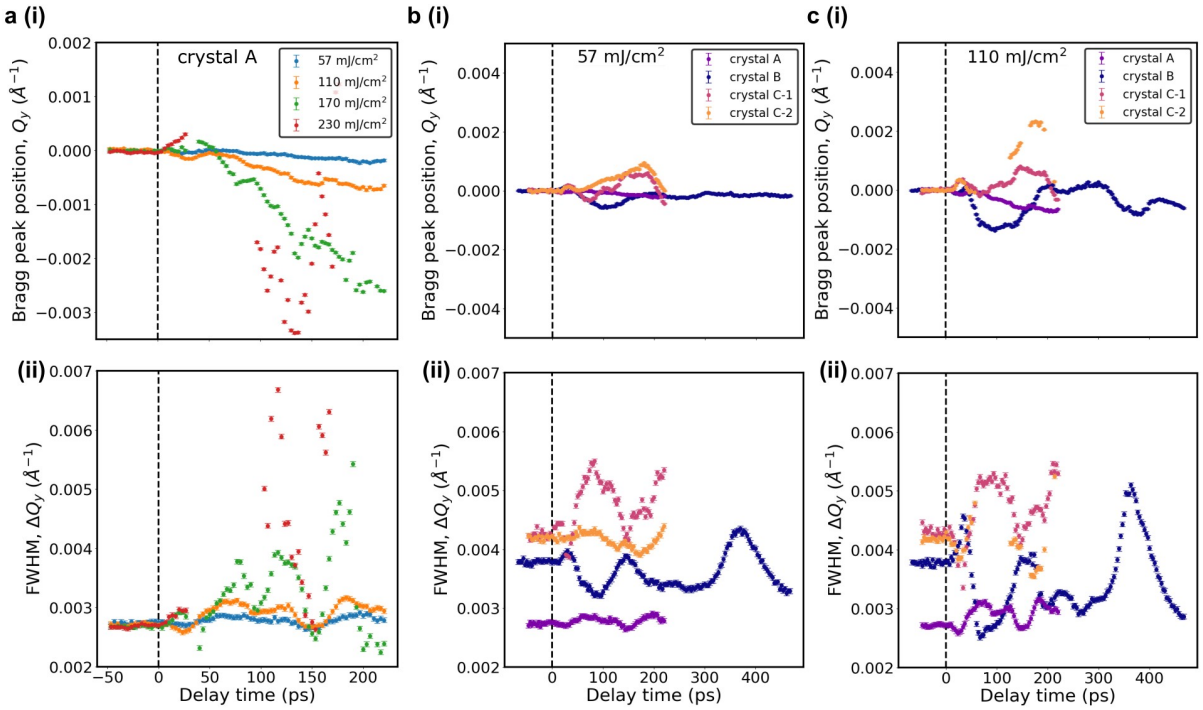

Figure S6: Summary of the changes to the Gaussian-fitted Bragg peaks along the Q_y (vertical) detector direction as a function of laser fluence and delay time. **a** Crystal A's fitted parameters for various laser fluences. (i) Fitted position of the Bragg peak along the vertical Q_y direction. The oscillations were fitted with Eq. S1 for all fluences except for 230 mJ/cm^2 due to a lack of signal. (ii) Fitted FWHM of the Bragg peak along the vertical direction. The oscillations were fitted with Eq. S2. **b** Fitted parameters for a laser fluence of 57 mJ/cm^2 on all measured crystals. **c** Fitted parameters for a laser fluence of 110 mJ/cm^2 on all measured crystals. Crystal C-1 and C-2 are two successive measurements on the same crystal. The error bars reflect two standard deviations of repeated measurements at negative delay times. The error of the Gaussian fits is shown in Fig. S9 for **b** and **c**. The equivalent of this figure in the Q_x direction is Fig. 3.

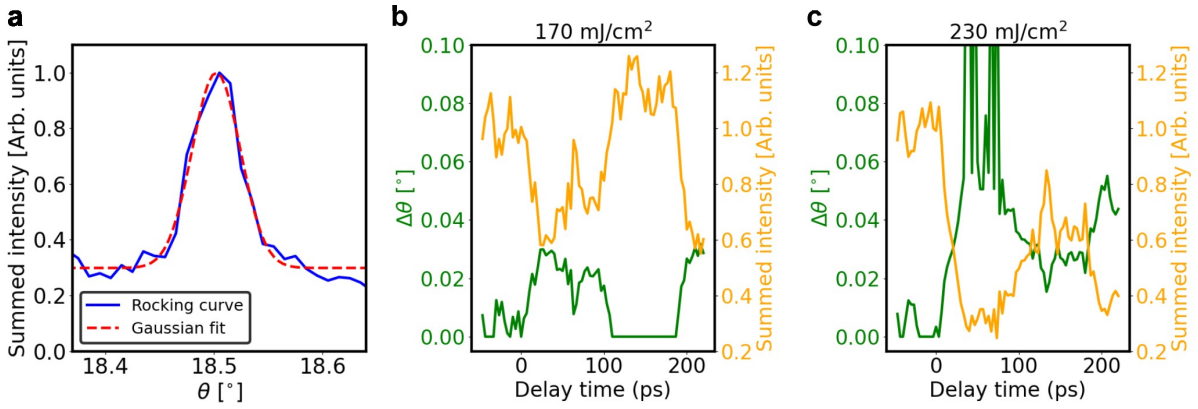

Figure S7: Estimation of rotation around the θ rocking axis for crystal A at high laser fluences based on the normalised summed intensity of the Bragg peak cropped to a 64×64 array. **a** The rocking curve for crystal A with a fitted Gaussian function used to compute the magnitude of θ rotation. **b** The rotation, given by theta deviation, $\Delta\theta$, for 170 mJ/cm^2. **c** The rotation for 230 mJ/cm^2. The summed intensity for **b** and **c** is normalised to the average summed intensity at negative delay times.

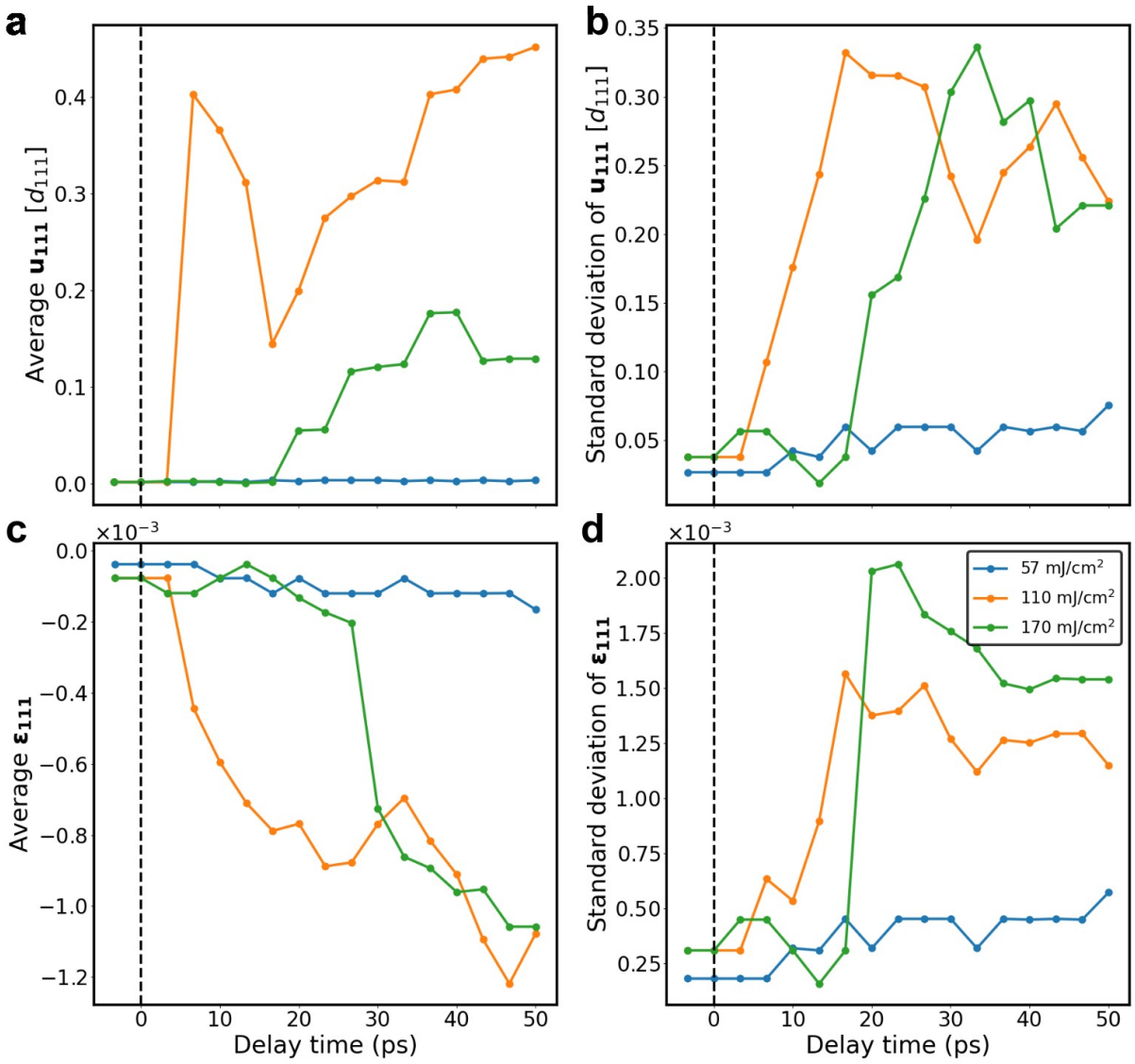

Figure S8: Additional displacement and strain trends for the 2D model of crystal A in Fig. 4. Displacement trends are shown for **a**, the mean $\mathbf{u_{111}}$, and **b**, the standard deviation of $\mathbf{u_{111}}$. Strain trends are shown for **c**, the mean ε_{111}, and **d**, the standard deviation of ε_{111}.

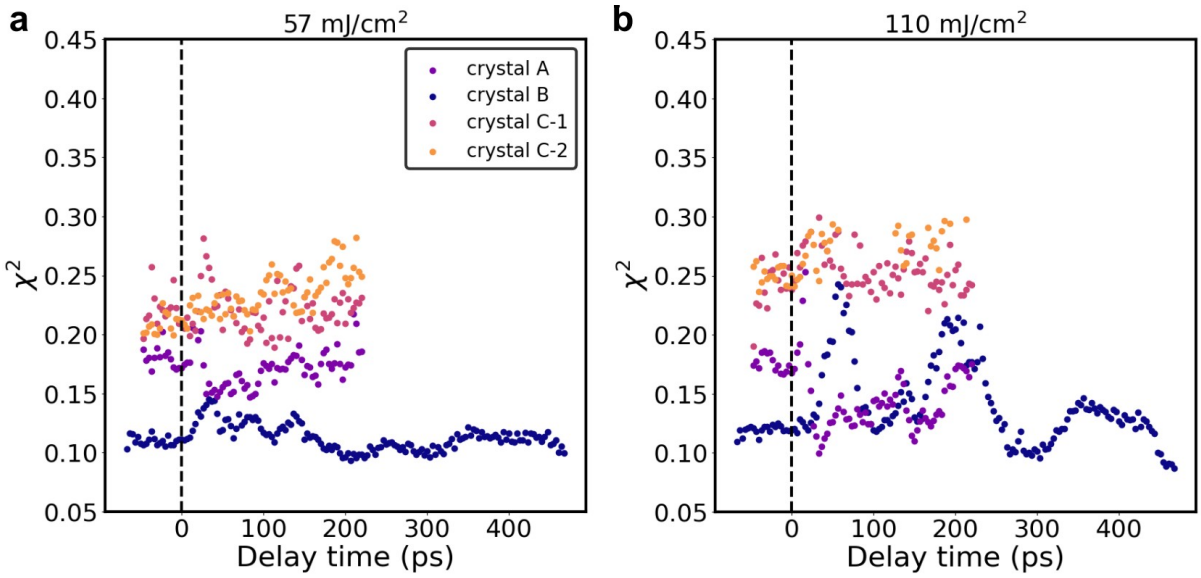

Figure S9: The χ^2 error of the Gaussian fit of the Bragg peak for multiple crystals at various delay times for **a** 57 mJ/cm^2 and **b** 110 mJ/cm^2. Each point corresponds to the fits shown in Figs. 3b and c and S6b and c.

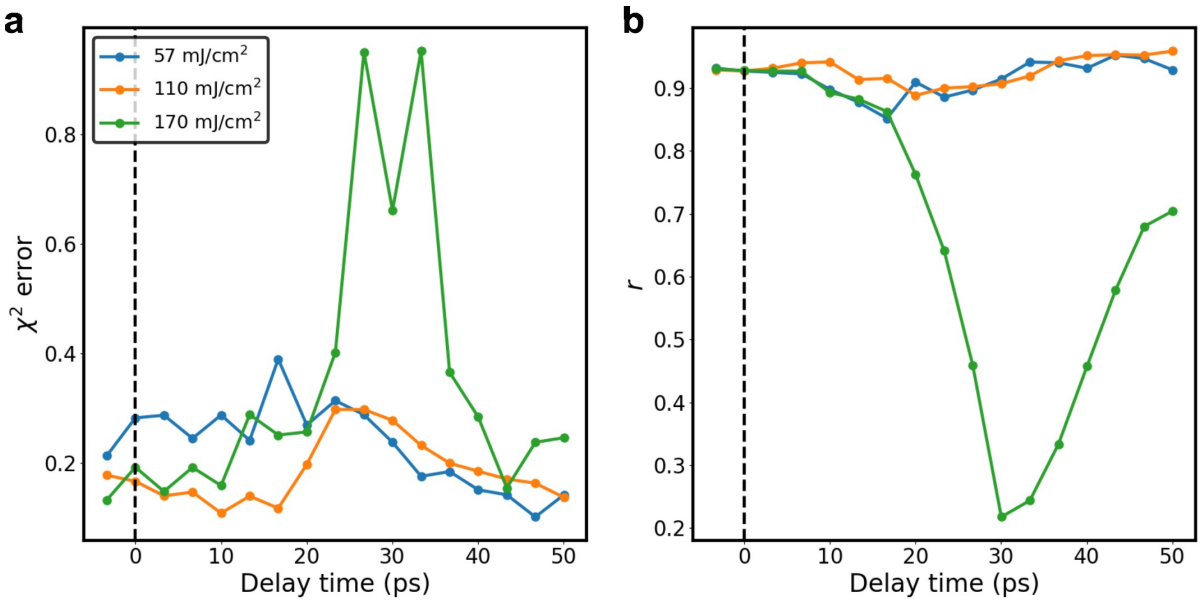

Figure S10: Comparison between the normalised Bragg peak of the model compared to the normalised experimental Bragg peak in Fig. 4. **a** The χ^2 error. **b** The Pearson correlation coefficient, r.

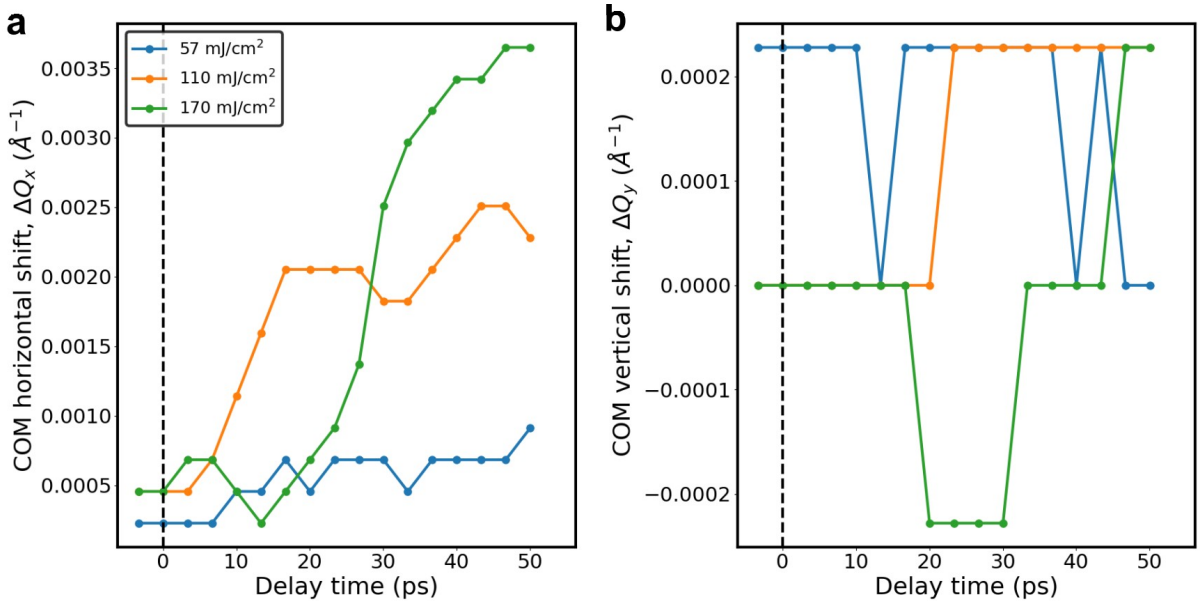

Figure S11: Additional centre of mass (COM) parameters used for the model in Fig. 4. These COM shifts of the model Bragg peaks were implemented separately and are shown for both **a**, the horizontal direction, ΔQ_x, and **b**, the vertical direction, ΔQ_y.

Table S1: Eq. S1 fitted parameters for Fig. 3a

mJ/cm^2	A_1	T_1	ϕ_1	A_2	T_2	ϕ_2	λ	C
57	2.5×10^{-2}	122	-9.9×10^{-2}	1.4×10^{-2}	61	-3.0	6.1×10^{-3}	2.8
110	4.9×10^{-2}	120	3.6×10^{-1}	3.0×10^{-2}	61	-2.7	1.1×10^{-2}	2.8
170	8.8×10^{-2}	120	1.3×10^{-1}	-5.0×10^{-2}	61	-6.0	1.1×10^{-2}	2.8

Table S2: Eq. S2 fitted parameters for Fig. 3d

mJ/cm^2	B	P	β	ζ	D
57	-9.4×10^{-4}	57	8.1×10^{-1}	1.9×10^{-2}	2.8×10^{-3}
110	-7.1×10^{-4}	58	1	0	3.5×10^{-3}
170	4×10^{-3}	58	1	0	7×10^{-3}